RSC Advances

PAPER

View Article Online
View Journal | View Issue

Cite this: *RSC Adv.*, 2024, **14**, 26505

Superhydrophobic stretchable sensors based on interfacially self-assembled carbon nanotube film for self-sensing drag-reduction shipping†

Shuai Wang, [ac] Weili Deng [b] and Weiqing Yang *[ab]

Multifunctional flexible electronics integrated with superhydrophobicity and flexible sensing can greatly promote broader applications. However, the hierarchical roughness morphology of superhydrophobic surfaces is vulnerable to complex mechanical deformations of stretchable sensors leading to degradation of hydrophobic properties, so constructing robust superhydrophobic stretchable sensors remains challenging. Herein, we propose a facile strategy to fabricate superhydrophobic stretchable sensors based on self-assembled carbon nanotube (CNT) films at the air–water interface. The customizable functions of superhydrophobic stretchable sensors can be achieved by controlling the combination of the CNT film and polydimethylsiloxane (PDMS) through a simple and efficient interfacial transferring strategy. Even under large mechanical deformations, the developed sensors can present excellent robustness and superhydrophobicity with a water contact angle of 150.9° at 80% strain. As a proof-of-concept, this work demonstrates their potential application in self-sensing drag-reduction shipping, which is expected to realize greener, more sustainable and safer aquatic transportation.

Received 2nd July 2024
Accepted 15th August 2024

DOI: 10.1039/d4ra04793a

rsc.li/rsc-advances

1. Introduction

Multifunctional flexible electronics can maximize the synergy effect of different types of single-function devices, which significantly broaden their application scenarios.[1–3] Nature provides endless bionic inspiration for the design of multifunctional flexible electronics. The superhydrophobic property of lotus leaves is a fascinating phenomenon, enabling the leaves not to be stained by the muddy environment, thus showing self-cleaning performance.[4,5] In addition, the skins of many animals have excellent stretchable sensing functions.[6–11] For example, human skin has excellent stretchability and multi-stimulus (pressure, temperature, humidity, *etc.*) sensing performance. Integrating the water-repellent function of superhydrophobic surfaces and the sensing function of stretchable sensors, superhydrophobic stretchable sensors can be obtained, which is of great value for a wide variety of applications.[12–14] For instance, waterproof stretchable sensors show improved anti-interference performance, expanding the application scope from dry environments to aquatic environments.

The construction of superhydrophobic stretchable sensors needs to meet the following requirements simultaneously: (i) hierarchical surface structures; (ii) low surface energy; and (iii) good stretchability. Stretchability of the epidermal sensors is crucial for the high-quality collection of imperceptible signals. However, the change of characteristic dimensions of the hierarchical surface structures or irreversible damage to the surface morphology due to localized stress concentrations occurs during mechanical deformation (stretching or bending) of stretchable sensors, causing the degradation of superhydrophobic performance. Therefore, the rational design and fabrication of superhydrophobic stretchable sensors is still challenging.

Due to the advantages of simplicity and cost-effectiveness, the coating strategy is most commonly used to construct superhydrophobic stretchable sensors, including dip coating,[15,16] spin coating,[17] spray coating,[18] Meyer-rod coating[19] *etc.* A variety of superhydrophobic stretchable sensors have been fabricated through the rational materials selection and engineered device structures.[20–28] The active materials for sensing function, include metal nanomaterials,[29] carbon nanomaterials,[30] MXene materials,[31–33] conductive polymers,[34–36] *etc.*; The superhydrophobicity is realized by designing hierarchical surface structures of micro/nanomaterials (such as SiO_2, TiO_2, *etc.*) and low surface energy treatment using fluorinated reagents or nonfluorinated reagents;[37,38] Elastomeric polymers or geometrically designed structures are used to ensure flexible and stretchable properties.[39,40] For instance, Dong *et al.*[41] reported a superhydrophobic nonwoven textile sensor. A first conductive layer of carbon black nanoparticles/carbon

[a]*Research Institute of Frontier Science, Southwest Jiaotong University, Chengdu, 610031, PR China. E-mail: wqyang@swjtu.edu.cn*

[b]*School of Materials Science and Engineering, Southwest Jiaotong University, Chengdu, 610031, PR China*

[c]*Laboratory of Polymers and Composites, Ningbo Institute of Materials Technology and Engineering, Ningbo, 315201, PR China*

† Electronic supplementary information (ESI) available. See DOI: https://doi.org/10.1039/d4ra04793a

nanotubes hybrids by dip coating, and a second superhydrophobic layer of fluorinated titanium dioxide nanoparticles by spray coating were constructed on styrene–ethylene–butylene–styrene fibers. The sensors show excellent health monitoring performance and immunity to interference, including corrosive liquids, and mechanical stimuli. Lin *et al.*[42] reported a superhydrophobic strain sensor with a sandwich structure, in which a bonding layer of 3-(aminopropyl)triethoxysilane and a conductive layer of carbon nanotubes/graphene hybrids were formed on polydimethylsiloxane (PDMS) substrate by spray-coating, and were further decorated with fluorinated silver nanoparticles. Stable strain sensing capability against liquid interference and bacterial adhesion was demonstrated during mechanical deformation. However, the existing preparation strategies often involve designing and preparing various functional materials from the beginning to construct an integrated flexible electronic device, which lead to complex and time-consuming preparation processes and unstable interfaces between different materials. In addition, uneven dispersion of active nanomaterials in the coating solution will cause poor performance. Therefore, the efficient, cost-effective construction of stable superhydrophobic stretchable sensors still needs to be further explored.

Herein, we propose a mild and efficient way to construct superhydrophobic stretchable sensors based on interfacially self-assembled carbon nanotube (CNT) films. Customizable functions (superhydrophobicity, stretchable strain sensing) based on one single material system of CNT/PDMS composite are achieved by controllable post-infiltration method. The semi-encapsulated CNT/PDMS (s-CNT/PDMS) composite is used to achieve excellent superhydrophobicity and surfaces with patterned wettability can be efficiently designed using a variety of substrate materials. The fully encapsulated CNT/PDMS (f-CNT/PDMS) composite features stretchable sensing for sensitive and stable monitoring of external strain stimuli. The superhydrophobic stretchable strain sensors are further fabricated from the integrated CNT/PDMS (i-CNT/PDMS) composite by exploiting the synergy between the customized individual functions. Finally, we successfully construct a high-performance artificial hovercraft and demonstrate the self-sensing hydrodynamic drag-reduction transportation, which is expected to promote energy-saving and safe aquatic transportation.

2. Experimental section

2.1 Materials and reagents

Multi-walled carbon nanotubes (diameter of 8–15 nm; length of 50 μm; amino content of about 0.45 wt%) with over 95% purity were acquired from Chengdu Organic Chemistry Co. Ltd Sylgard 184 silicone elastomer kit was supplied by Dow Chemical company (USA). Anhydrous ethanol and *n*-hexane were purchased from Sinopharm Chemical Reagent Co., Ltd and used as received. Silver pastes, copper wires were purchased from SPI company (USA) and Baihong Wire (Shenzhen) Co., Ltd, respectively. Polyethylene terephthalate (PET) sheets, polyimide (PI) films were obtained from Ocan polymer company and DuPont company, respectively.

2.2 Fabrication of the functional composite films and devices

2.2.1 Preparation of the interfacially self-assembled CNT film. A modified Langmuir–Blodgett method was used to prepare the self-assembled CNT film. Briefly, multi-walled carbon nanotubes were dispersed into anhydrous ethanol (0.3 mg mL^{-1}) and ultrasonication (200 W) was applied for 1 h (Scientz-IID, Scientz Co., Ltd). Then the multi-walled carbon nanotubes/anhydrous ethanol solution (50 mL) was sprayed onto the water surface (700 cm^2) by a spray gun. A uniform pre-assembled multi-walled carbon nanotube film was formed at the air–water interface. A piece of microporous sponge was put into the water at one side of the interface. The carbon nanotubes at the air–water interface then receded away from the sponge block and a closely stacked carbon nanotube assembly layer was formed until the area of the assembly film could not be condensed further.

2.2.2 Controllable fabrication of the CNT/PDMS composite films. The air–water interfacially self-assembled CNT film was transferred onto a solid substrate by inserting the substrate with a tilted angle in the water and then slowly approaching the film. The wet CNT film transferred to the substrate was dried by nitrogen flow at room temperature to obtain a uniform CNT film on the substrate. Next, controlled preparation of CNT/PDMS composite films were conducted. The PDMS prepolymer (10 : 1 ratio of the main agent and crosslinker) was diluted to 5% mass fraction with hexane and dispersed homogeneously by ultrasonication. The dispersion was sprayed onto the CNT film transferred on the solid substrate by a spray gun, and thermally cured to obtain s-CNT/PDMS composite coatings. The undiluted PDMS prepolymer (10 : 1 ratio of the main agent and crosslinker) was dropped on the CNT film transferred on the solid substrate. The paste was scraped uniformly on the surface of the CNT film and then thermal cured to obtain the f-CNT/PDMS composite films. The f-CNT/PDMS composite films were peeled off from the solid substrate. The f-CNT/PDMS composite film was used to further transfer the interfacially self-assembled CNT films, and the i-CNT/PDMS composite film was obtained after being treated as the same preparation process of the above s-CNT/PDMS composite samples.

2.2.3 Preparation of the superhydrophobic coatings and stretchable sensors. Multilayer self-assembled CNT films were transferred onto a solid substrate covered with patterned masks, and then sprayed with diluted PDMS prepolymer solution, followed by thermal curing to obtain the patterned superhydrophobic surfaces. The construction process was the same as the above for substrates of different material types and shapes. Powders were put on the superhydrophobic surface fabricated on a glass substrate and then flushed with water from above to verify the self-cleaning performance. The f-CNT/PDMS composite film was used to fabricate stretchable sensors by coating silver paste on two end sides along the length direction of the sample. Then fine copper wires were connected separately to the above silver pastes and dried by heating in an oven. The sensors were pre-stretched by the universal testing machine before the sensing performance characterization.

2.2.4 Fabrication of the artificial hovercraft. The artificial hovercraft was constructed by fixing the i-CNT/PDMS composite membrane under an empty plastic container with the aid of adhesive tapes, and certain spacing distance was maintained between the integrated composite film and the bottom of the container. External propulsive airflow was provided by rubber suction bulb. An object such as a piece of glass was placed into the hull of the artificial hovercraft to demonstrate the cargo transportation application on the water surface and electrical sensing signals were recorded in the meanwhile by the electrochemical workstation.

2.3 Characterization

The field emission scanning electron microscope (FE-SEM) images were acquired using a FE scanning electron microanalyzer (Hitachi-S4800, 4 kV). The microscopic optical images were obtained by optical microscopy (Olympus, BX 51TF Instec H601). Both transmission and reflection modes were used to acquire optical images. The mechanical property of the integrated composite film was measured by the universal testing machine (Instron 5567). The water contact angles on the sample surfaces were obtained by a Data physics OCA15Pro instrument (DataPhysics Instruments). Three different positions were measured to calculate the average contact angle. The method for measuring the sliding angles of the water droplet on the coating is as follows: the rotation speed is 90° min^{-1}, the maximum rotation angle is 30° and three different positions were measured to calculate the average value. Controlled tensile strains were exerted to the stretchable sensors using the universal testing machine (Instron 5567) and the electrical sensing signals of the devices under different tensile strain deformations were synchronously recorded by an electrochemical workstation (CHI760E, CH Instruments Inc).

3. Results and discussion

3.1 Design and fabrication strategy

Our design and fabrication strategy of superhydrophobic stretchable sensors is shown in Fig. 1. Interfacially self-assembled carbon nanotube (CNT) film was prepared by a modified Langmuir–Blodgett method according to our previous works.[43–45] In brief, the CNTs were dispersed in ethanol and the dispersion was atomized and sprayed onto the air–water interface. Based on the Marangoni effect, the CNT dispersion could be rapidly spread onto the air–water interface. Then successive interfacial compression was exerted on the pre-assembled CNT film using a piece of microporous sponge until the film area stopped shrinking, and the self-assembled CNT film at the air–water interface was finally obtained. Simple and convenient transfer of the interfacially self-assembled CNT film onto a solid substrate with specific shapes was conducted and the wet film was further dried to obtain a uniform CNT film on the transferred substrate (Fig. 1a).

Through controlled composite of the interconnected CNT networks and PDMS using post-infiltration method, we can realize customizable single functions based on the same CNT/PDMS composite material system. The stacking structure of the interfacially self-assembled CNT film is favorable for the infiltration of liquid PDMS prepolymer due to the gaps between one-dimensional CNTs with high aspect ratio (Fig. S1†). The s-CNT/PDMS composite exhibits superhydrophobic properties, but is not stretchable. The f-CNT/PDMS composite exhibits stretchable properties, which can be used for stretchable strain sensing, but it does not have superhydrophobic properties. Furtherly, through the convenient sequentially interfacially-transferring strategy, the i-CNT/PDMS composite enables the efficient integration of the above two functional layers and thus is used to construct the superhydrophobic stretchable strain sensor (Fig. 1b). The Young's modulus of the integrated composite film is 877 kPa (Fig. S2†). The soft mechanical property ensures both wearing comfort and stable sensing performance. Based on the robust fabrication processes, despite the multi-step fabrication process, the obtained samples exhibit the consistent structures and performances. The continuous distribution of silicon elements between the upper and lower layers indicates the formation of an interpenetrating polydimethylsiloxane polymer network, which ensures a seamless and stable interface between the different layers (Fig. S3†). The constructed structure can thus facilitate the consistent performance of the fabricated samples. Notably, the approach here has lots of advantages: The superhydrophobic layer and the conductive layer of the integrated composite film are interpenetrated by the same PDMS polymer network, which avoids the design and fabrication of additional bonding materials in previous studies, ensuring more compatible and stable interface. Meanwhile, the PDMS is utilized for the low-surface-energy modification. What's more, the self-assembled CNT films not only endow the integrated composite film with the hierarchical surface structures to realize the superhydrophobic performance, but also provide the electrical conductivity derived from the interconnected conductive CNT networks required for the stretchable sensing function. The integrated composite film exhibits synergistic properties of stretchable sensing performance enabled by the elasticity of the fully encapsulated layer and superhydrophobicity enabled by the surface roughness of the semi-encapsulated layer, which can be used for unique application scenarios such as self-sensing hydrodynamic drag reduction shipping in aquatic environments (Fig. 1c).

3.2 Customizable single functions based on interfacially self-assembled CNT film

Customizable single functions were realized based on interfacially self-assembled CNT film. In terms of constructing superhydrophobic surface, diluted PDMS prepolymer solution was spray-coated onto the self-assembled CNT film and cured by heating to obtain s-CNT/PDMS composite coating. Fig. 2a–c shows that the s-CNT/PDMS composite coating retained the surface roughness morphology of self-assembled CNT films derived from random stacking of one-dimensional CNTs and the PDMS polymer with low surface energy partially wrapped the CNTs, which synergistically contributed to

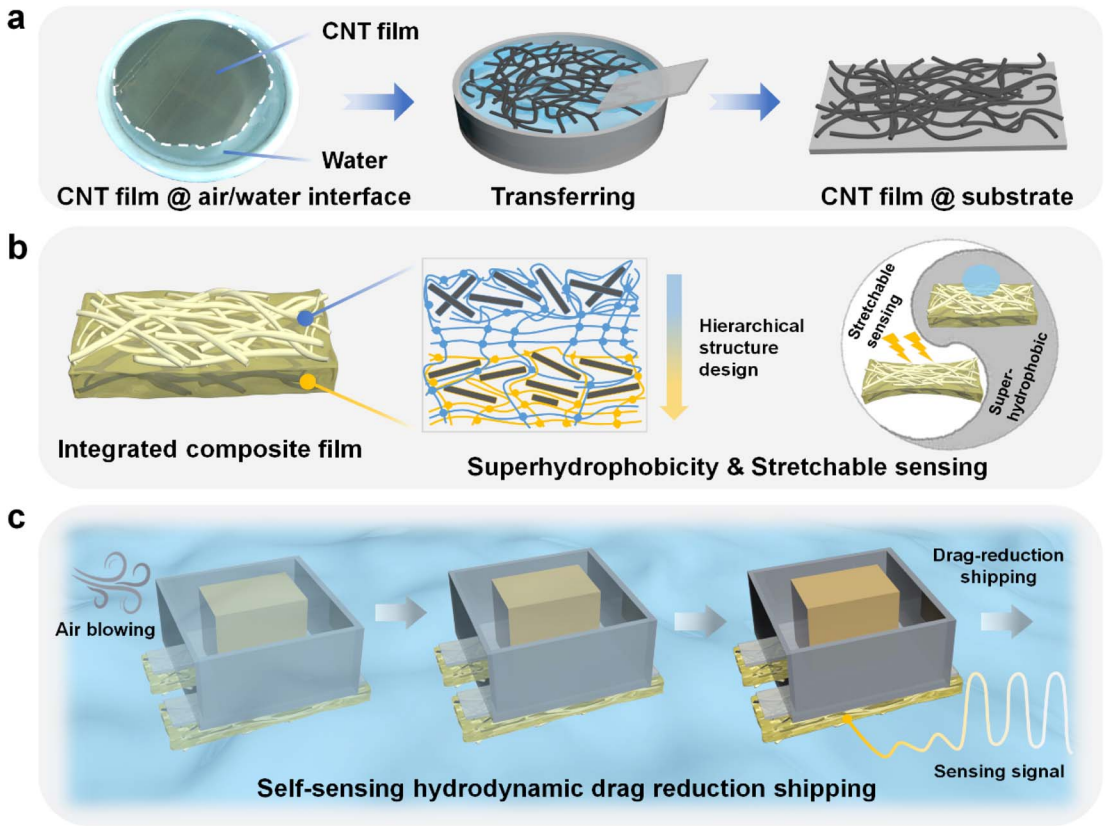

Fig. 1 Design and fabrication strategy of superhydrophobic stretchable sensor based on interfacially self-assembled CNT films. (a) Preparation and transferring of the self-assembled CNT film at air/water interface. (b) The integrated composite films with hierarchical structure design were efficiently fabricated by combining the customized individual functions to achieve superhydrophobic stretchable sensing performance. The self-assembled CNT film partially encapsulated by polydimethylsiloxane was designed to obtain superhydrophobic property. The self-assembled CNT film fully encapsulated by polydimethylsiloxane was designed to obtain stretchable sensing property. (c) The self-sensing hydrodynamic drag reduction shipping application can be realized by using the integrated composite film.

a superhydrophobic surface. The wettability of s-CNT/PDMS coatings can be effectively regulated by the transferring layers of interfacially self-assembled CNT films (Fig. 2d). The water contact angles (WCA) of s-CNT/PDMS coatings increase significantly with the transferred CNT film layers. From the contact angle test images, it can be seen that superhydrophobicity begins to appear when the film is 4 layers or more and its WCA exceeds 150°. We measured the water sliding angle of the samples. The four-layer sample exhibited a rolling angle of 6.3°, and the five-layer sample exhibited a rolling angle of 4.2°, while for the samples with less than four layers, even when the test platform was tilted beyond 10°, no water droplet rolling occurred. The camera was positioned parallel to the test substrate plane where the droplet was added, and the rolling processes of the water droplet on the superhydrophobic surfaces were recorded, as shown in Fig. S4.† To compare the morphologies of the films with different layers, we performed morphological characterizations using SEM for different samples. As the transfer layer number of the CNT film increased, the composite film progressively formed a semi-encapsulated CNT/PDMS structure with more one-dimensional nanotubes exposed on the surface, creating a hierarchical rough surface morphology that facilitates the realization of superhydrophobic sensing performance (Fig. S5†). In addition, through the mask-assisted interfacial transfer strategy, we can easily design material surfaces with patterned wettability properties (Fig. 2e). By selectively transferring multiple layers of self-assembled CNT films to the hollow area of the masks, we can obtain customized butterfly and Christmas tree patterns, which exhibit patterned superhydrophobic surfaces after low surface energy treatment. This can be verified by the silver mirror phenomenon formed by the light refraction of the air layer trapped at the superhydrophobic surface when submerged in water. The patterning strategy will enable great flexibility to design in practical applications. The water droplets rolled off the superhydrophobic surface by tilting the sample and the change of the water jet direction on the superhydrophobic surface like light reflection were also observed from Fig. S6,† which confirm the reliable and excellent superhydrophobic performance.

The construction strategy is applicable to both flat substrates and curved substrates. We used the side of a cylindrical container to transfer the air–water interfacially self-assembled CNT film. The curved surface was uniformly covered by the self-assembled CNT film and then treated with low surface energy reagents using PDMS. The silver-mirror phenomenon of

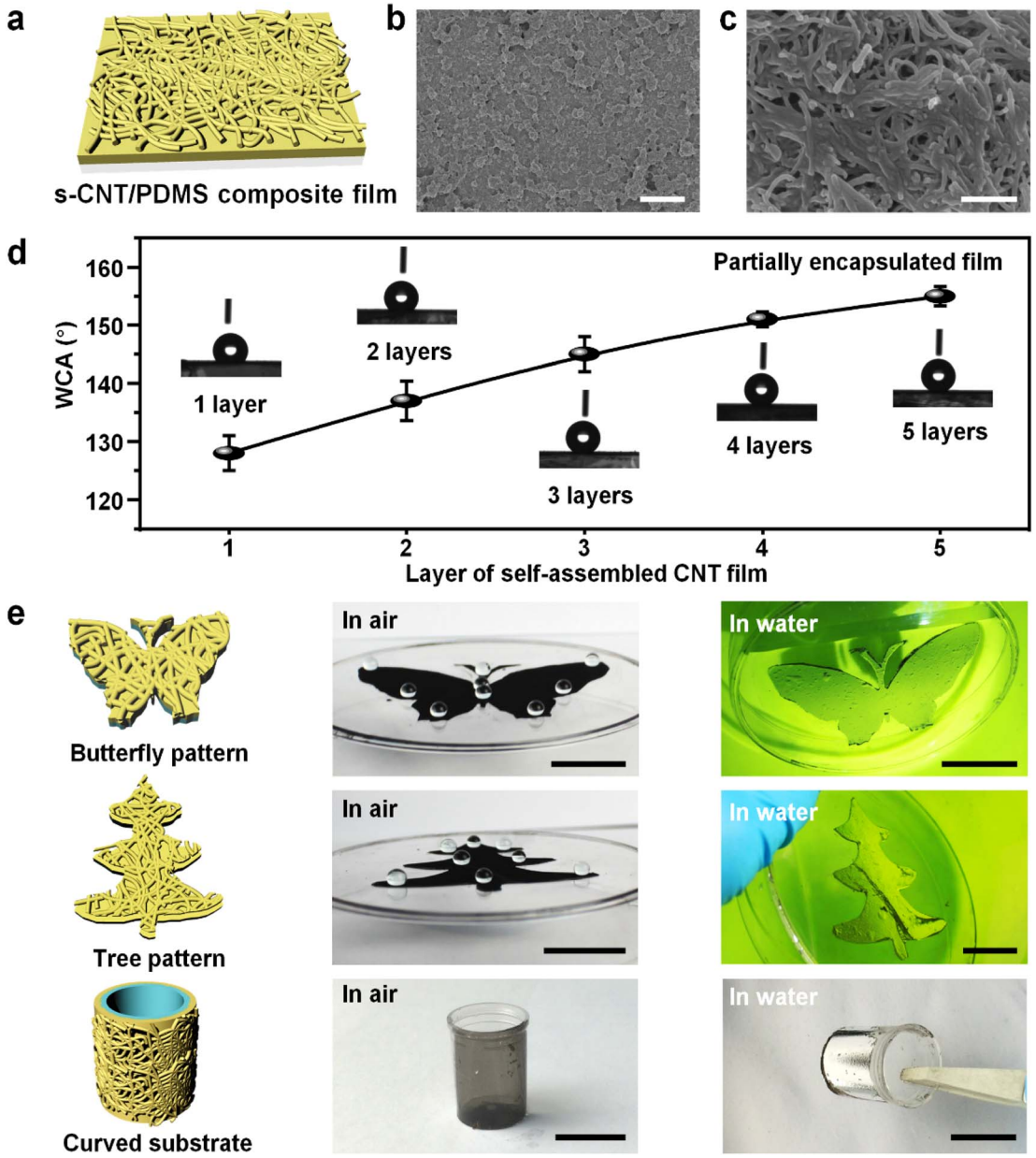

Fig. 2 Superhydrophobic surfaces based on s-CNT/PDMS composite films. (a) The illustration of the surface morphology of the s-CNT/PDMS composite film. (b and c) SEM images of the surface morphology of the s-CNT/PDMS composite film. Scale bars: 20 μm (b), 500 nm (c). (d) Change of the WCA of s-CNT/PDMS composite films with the transferred layer of self-assembled CNT films. (Insets): Typical images of water droplets on the surfaces of s-CNT/PDMS composite films. (e) Patterned superhydrophobic surfaces constructed on both flat substrates and curved substrates. Scale bar: 2 cm.

the curved superhydrophobic surface can also be observed in water. In addition, our construction strategy can be applied to a wide variety of materials. The CNT film at the air–water interface can be efficiently transferred to the surfaces of polymer substrates (PDMS, polystyrene, *etc.*), metal substrates (tin foil, *etc.*), and inorganic non-metallic substrates (glass, *etc.*) (Fig. S7†). The original hydrophilic surfaces of glass, tin foil and hydrophobic surfaces of PDMS, polystyrene can be efficiently converted into superhydrophobic surfaces (Fig. S8 and Table S1†). We placed some powders on the s-CNT/PDMS coating surface and then poured water onto the surface. It was observed that the powders on the substrate surface had been carried away by the water flow, proving the self-cleaning performance (Fig. S9†). This self-cleaning mechanism is that the bonding force between the dust and the water flow on the superhydrophobic surface is larger than that between the dust and the coating surface, so the pollutants are removed by flowing water easily. These results show that our construction strategy of superhydrophobic property is highly efficient, which greatly facilitates the future applications.

To realize stretchable sensing, the PDMS prepolymer was dropped onto the self-assembled CNT film and thermally cured

to fabricate the f-CNT/PDMS sensor. The morphology of the f-CNT/PDMS composite film was investigated. The CNTs were all encapsulated in the PDMS matrix, presenting flat surface morphology, which can be seen in Fig. S10.† The good encapsulated composite structure enables the composite film to be free-standing and stretchable. The f-CNT/PDMS composite film consists of two layers: the upper layer is the conductive self-assembled CNT film encapsulated in an insulating PDMS matrix with piezoresistive sensing characteristics and the lower layer is pure PDMS that serves to ensure the property of elasticity. We then studied the electromechanical performance of the f-CNT/PDMS strain sensors (Fig. 3a). The sensitivity of the stretchable strain sensors is evaluated by gauge factor (GF). The GF is calculated by the equation $GF = (\Delta R/R_0)/(\Delta L/L_0) = (\Delta R/R_0)/\varepsilon$, where ΔR is the change of the resistance, R_0 is the initial resistance, ΔL is the change of length, L_0 is the initial length, and ε is the tensile strain. Fig. 3b shows the sensing performance of the f-CNT/PDMS strain sensor. The relative resistance increased rapidly with applied strain in the initial stage (GF_1: 40, strain of 10–25%) and then increased slowly subsequently (GF_2: 6, strain of 45–80%). In the initial stage, the applied strain stimulus was partly absorbed to pre-tighten the stretchable sensing device. As a result, the actual strain transmitted to the composite film was reduced, leading to a relatively weaker sensing response of the device during this stage. It's worth noting that the f-CNT/PDMS strain sensor shows good linearity in both sensing stages, which helps simplify the data analysis process and is beneficial for practical sensing applications. The sensing mechanism is that the resistances vary with externally applied strains due to the reversible opening–closing of microcracks in the f-CNT/PDMS composite film (Fig. S11†). In the first sensing stage, the microcracks opened and conductive pathways reduced rapidly accordingly, thus resulting in a larger GF in the beginning. In the second sensing stage, most microcracks had already opened without new microcracks, resulting in a relatively slow increase of electrical resistance with lower GF. The relative resistance

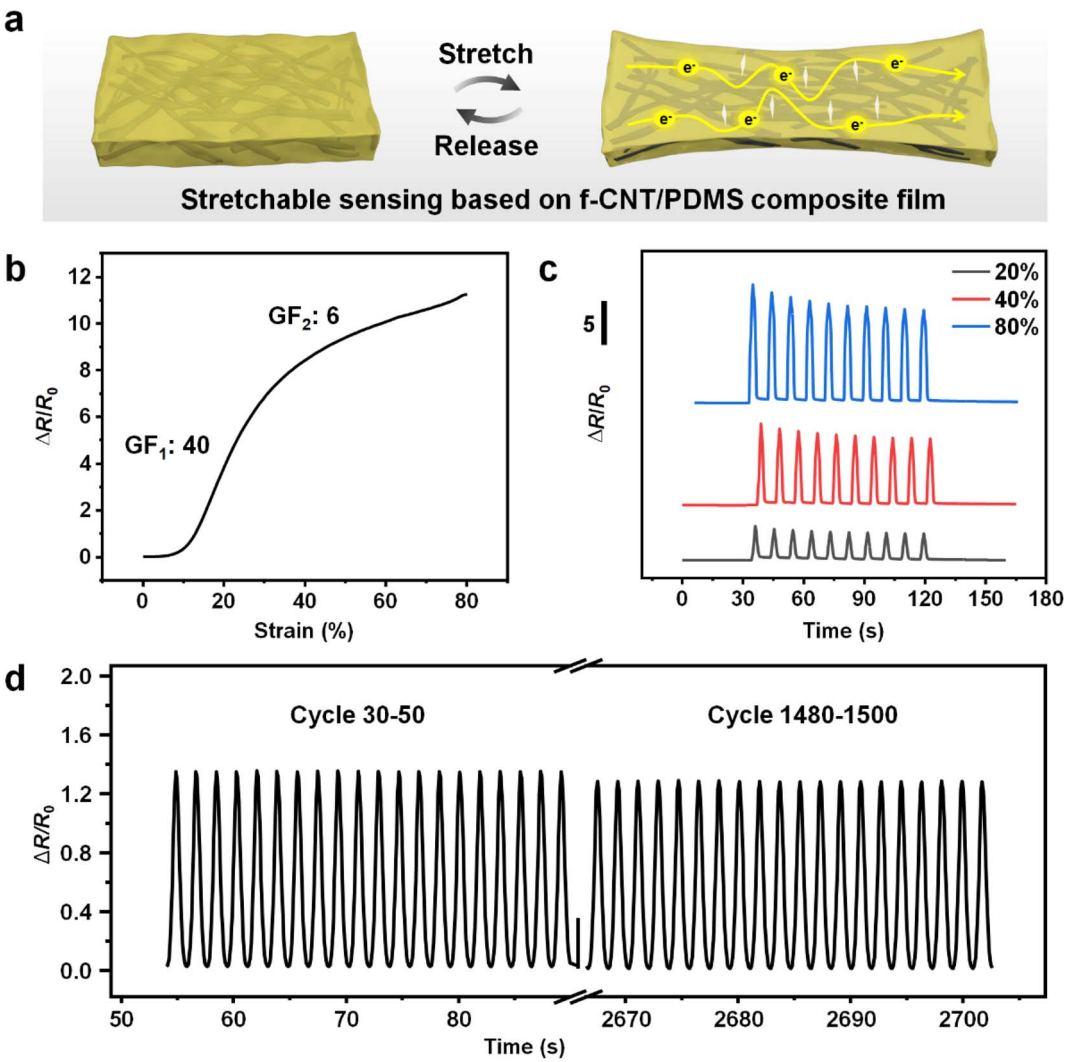

Fig. 3 Stretchable strain sensors based on the f-CNT/PDMS composite film. (a) The electromechanical performance characterization of the f-CNT/PDMS strain sensors. (b) Relative resistance of the f-CNT/PDMS strain sensors as a function of tensile strain. (c) Dynamic electrical response of the f-CNT/PDMS strain sensor to cyclic loading and unloading tensile strain of 20%, 40%, 80%. (d) Durability characterization of the f-CNT/PDMS strain sensor.

change under cyclic loading and unloading tensile strain of 20%, 40%, 80% is shown in Fig. 3c, demonstrating stable signal responses. Fig. S12† shows a response time of 92 ms and a recovery time of 917 ms. The relatively longer recovery time is due to the hysteresis of polymer chain movements in the polymer matrix. The excellent long-term stability and reliability of the f-CNT/PDMS strain sensor is shown in Fig. 3d. The testing results demonstrate that the f-CNT/PDMS composite film can be used in stretchable sensing applications.

3.3 Multifunctional integration of superhydrophobicity and stretchable sensing

Multifunctional integration of superhydrophobicity and stretchable sensing in the i-CNT/PDMS composite film was achieved through a simple sequentially interfacial-transferring strategy. Considering that the fine hierarchical structures of superhydrophobicity are vulnerable to mechanical deformations, the key to realize the integration of superhydrophobicity and stretchable sensing is to ensure that there is no crosstalk between superhydrophobicity and stretchability. The surface wettability change of the i-CNT/PDMS composite film under stretching conditions was investigated (Fig. 4a). We stretched the samples at different tensile strains (0%, 20%, 40%, and 80%) and then submerged them in water. The silver mirror phenomena due to trapped air of the superhydrophobic surface were observed for all the samples under different tensile strains, which suggests that the superhydrophobic property can be maintained under stretching deformations (Fig. 4b and c). Further, we measured the WCA quantitatively to describe the surface wettability change under the tensile strain conditions more accurately. From Fig. 4d, it can be seen that the WCA was 152.6° at 0% strain and 150.9° at 80% strain, with a slight

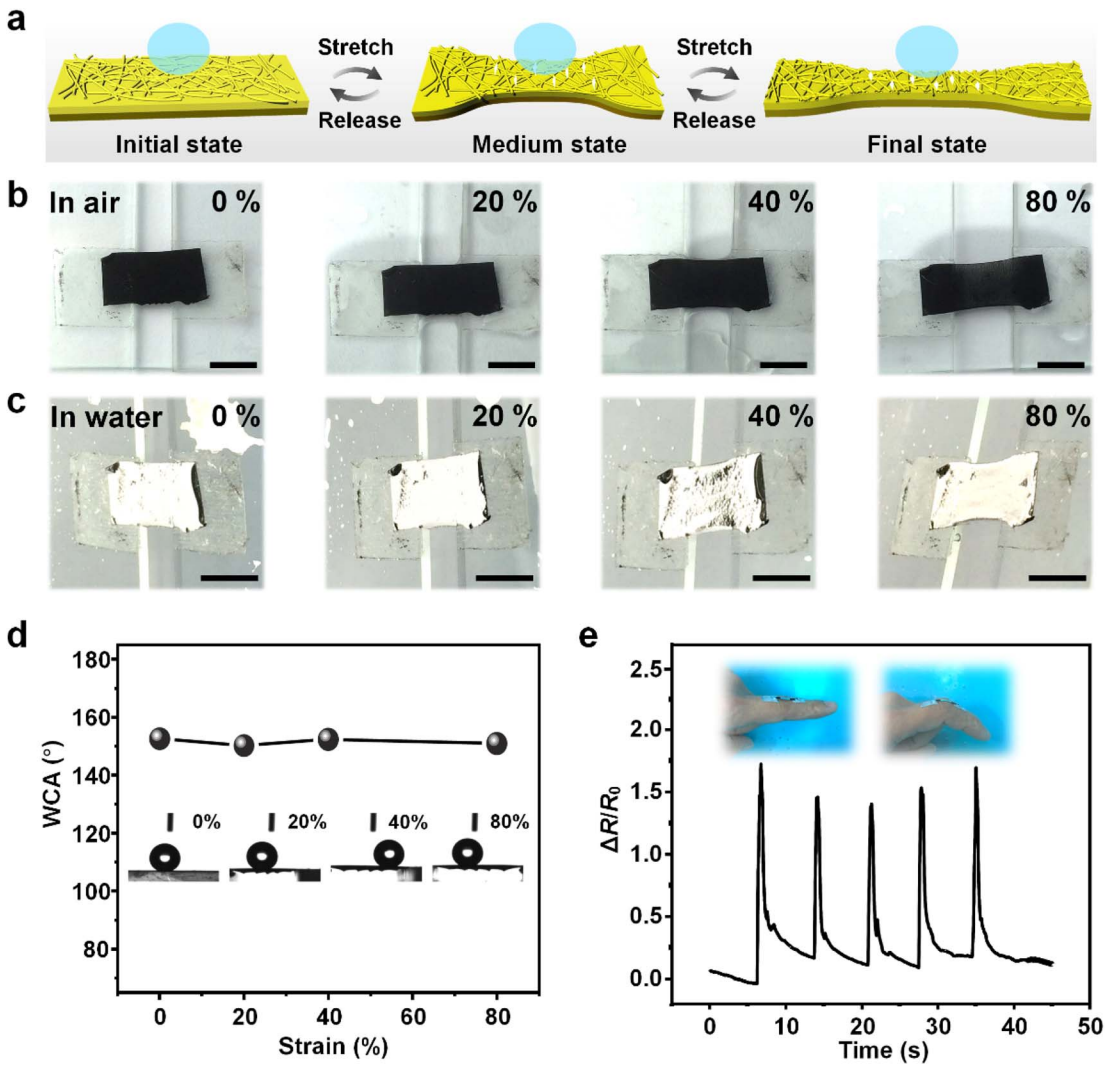

Fig. 4 Integration of superhydrophobicity and stretchable sensing properties based on the i-CNT/PDMS composite film. (a) Illustration of the surface wettability investigation of the i-CNT/PDMS composite film under stretching deformations. (b and c) Optical photographs showing the sample stretched at different tensile strains (0%, 20%, 40%, and 80%) and then submerged in water. Scale bar: 5 mm. (d) The WCA change of the i-CNT/PDMS composite film *versus* tensile strains. (Insets): Typical images of water droplets on the surfaces of i-CNT/PDMS composite films under stretching deformations. (e) Stable monitoring of the finger bending motions underwater by the superhydrophobic sensor. An obvious silver mirror phenomenon can be observed on the active part of the sensor.

decrease in WCA. This is because the sample was stretched longitudinally while being compressed laterally due to the Poisson effect during stretching, resulting in a slight decrease in surface roughness of the film. In addition, the low-surface-energy PDMS coating remained stable during the stretching process due to the robust crosslinked polymer network structure. Therefore, the composite film remains superhydrophobic up to a strain of 80%. The absence of crosstalk between the superhydrophobicity and stretchability of the i-CNT/PDMS composite film lays a solid foundation for practical applications. We conducted additional experiments to demonstrate the strain sensing performance of the superhydrophobic strain sensor in water environments. The superhydrophobic sensor was adhered to the finger joint and then submerged underwater. The active part of the superhydrophobic sensor trapped a uniform air layer underwater, exhibiting the silver mirror phenomenon due to light refraction. This excellent performance enabled the sensor to stably monitor finger bending motions in the water environment (Fig. 4e).

3.4 Self-sensing hydrodynamic drag reduction shipping application

Taking unique advantages of the superhydrophobicity property and stretchable sensing function of the i-CNT/PDMS composite film, self-sensing hydrodynamic drag reduction shipping in aquatic environment is demonstrated. Hovercraft is a kind of ship that relies on the high-pressure air generated by the blower

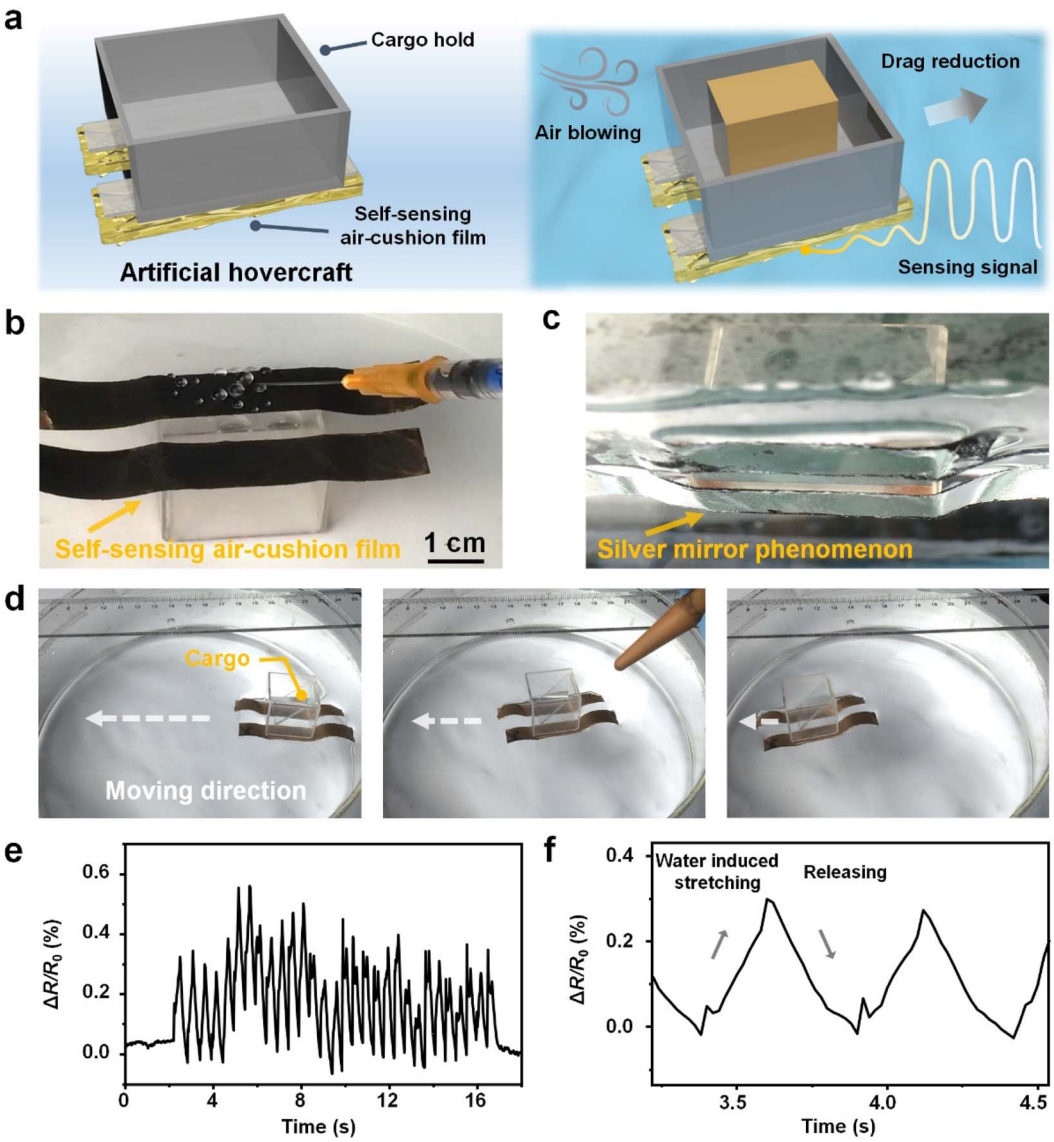

Fig. 5 Self-sensing hydrodynamic drag reduction shipping application of the artificial hovercraft based on the i-CNT/PDMS composite film. (a) The artificial hovercraft assembled from the i-CNT/PDMS composite film as a bottom support and a cargo-carrying hull fixed upon the composite film. (b) The artificial hovercraft was turned over to observe the superhydrophobic surface. (c) The artificial hovercraft can successfully float on the water surface enabled by the air cushion trapped by the superhydrophobic surface of the integrated composite film. (d) Drag-reducing cargo transportation of the artificial hovercraft loaded with a piece of glass slide on the water surface propelled by external airflow. (e and f) Self-sensing signals of the artificial hovercraft during sailing.

to form a cushion of air between the hull of the ship and the water surface, so that the hull of the ship is detached from the support surface for sailing. Unlike existing hovercrafts that require additional energy to maintain the air cushion, we can construct an artificial hovercraft based on the i-CNT/PDMS composite film. The superhydrophobic surface of the composite film can trap air pockets automatically between the hierarchical roughness structures with no need for external energy consumption when submerged in water, which is a unique advantage compared to the current commercial hovercraft.

We utilized the i-CNT/PDMS composite film as a bottom support for the artificial hovercraft, which can be used as a self-sensing air cushion film. A cargo-carrying hull is assembled upon the composite film, and then we investigated its self-sensing drag-reduction transportation on the water surface (Fig. 5a). Due to the increased buoyancy and reduced hydrodynamic frictional drag resistance brought about by the air cushion trapped by the superhydrophobic surface of the i-CNT/PDMS composite film, the artificial hovercraft can successfully float on the water surface without sinking (Fig. 5b and c). By blowing the artificial hovercraft with the external airflow, the artificial hovercraft started to move forward. The hull can also be loaded with cargo (a piece of glass slide) to carry out the cargo transportation on the water surface, as demonstrated in Fig. 5d. The artificial boat without the superhydrophobic surface, by contrast, sank easily (Fig. S13†). Meanwhile, the above navigation and transportation process can be monitored in real-time by the i-CNT/PDMS composite film. When the airflow impacts the hull, the reaction force of the water surface causes an increase in the relative resistance of the i-CNT/PDMS composite film fixed at the bottom of the ship. The reaction force disappears when the airflow is removed, and the relative resistance is restored to the original level. The electrical sensing signals provide crucial information of the sailing status to ensure the safe transportation on the water surface (Fig. 5e and f). Our exploration will help to advance the development of a new type of shipping transportation technology, which will greatly save fossil fuel consumption to promote the realization of a low-carbon and sustainable future and ensure the transportation safety.

4. Conclusions

A facile method was developed to fabricate superhydrophobic stretchable sensors utilizing air–water interfacially self-assembled CNT film. Customizable design of the single-function composite materials can be efficiently realized *via* a controllable combination of self-assembled CNT film and PDMS. The s-CNT/PDMS superhydrophobic coatings can be efficiently constructed on substrates of various materials and shapes. Patterned wettability of the surfaces was achieved *via* mask-assisted interfacial transfer. The f-CNT/PDMS stretchable sensors exhibit excellent strain sensing performance with good linear characteristics and stable cycling stability. Furthermore, the superhydrophobic stretchable sensors were obtained by integrating the above single functions through the sequentially interfacial transfer strategy. The i-CNT/PDMS composite films show excellent robustness with superhydrophobicity even under large stretching deformations. Compared with previous studies, the advantage of our approach is the construction of multifunctional integrated electronics based on a single CNT/PDMS composite system, which avoids the complicated and time-consuming preparation process involving various functional materials. The self-assembled CNT film not only endows the composite film with micro- and nanostructures required for superhydrophobicity, but also enables sensing functionality due to the interconnected conductive network. The PDMS not only serves as an interpenetrating polymer network connecting the two functional layers to ensure interface stability, but also is employed as low-surface-energy materials for superhydrophobicity. A self-sensing drag reduction transportation of an artificial hovercraft was finally demonstrated based on the synergy of hydrodynamic drag-reduction, waterproofness and flexible sensing properties of the i-CNT/PDMS composites. This strategy provides new ideas for developing novel superhydrophobic stretchable devices and promotes the development of more energy-efficient and safer shipping in the future.

Data availability

The data supporting this article have been included as part of the ESI.†

Author contributions

Shuai Wang: conceptualization, methodology, investigation, data curation, formal analysis, visualization, writing – original draft, funding acquisition. Weili Deng: funding acquisition, resources, writing – review & editing. Weiqing Yang: conceptualization, writing – review & editing, project administration.

Conflicts of interest

There are no conflicts to declare.

Acknowledgements

This research was financially supported by the Postdoctoral Fellowship Program of CPSF under Grant Number GZC20232184, the Fundamental Research Funds for the Central Universities (2682024CX075),China Postdoctoral Science Foundation (Certificate Number: 2024M752672), Sichuan Science and Technology Innovation Seedling Project Cultivation Program (24PYXM1687), the Natural Science Foundation of Sichuan Province of China (No. 2023NSFSC0313), and the Basic Research Cultivation Project of Southwest Jiaotong University (No. 2682023KJ024).

Notes and references

1 M. Lin, Z. Zheng, L. Yang, M. Luo, L. Fu, B. Lin and C. Xu, *Adv. Mater.*, 2021, **34**, 13.
2 Z. Ma, X. Xiang, L. Shao, Y. Zhang and J. Gu, *Angew. Chem., Int. Ed.*, 2022, **61**, 9.

3 H. Wang, S. Li, H. Lu, M. Zhu, H. Liang, X. Wu and Y. Zhang, *Small Methods*, 2023, **7**, 21.
4 S. S. Latthe, R. S. Sutar, V. S. Kodag, A. K. Bhosale, A. M. Kumar, K. Kumar Sadasivuni, R. Xing and S. Liu, *Prog. Org. Coat.*, 2019, **128**, 52.
5 X. Su, H. Li, X. Lai, Z. Yang, Z. Chen, W. Wu and X. Zeng, *J. Mater. Chem. A*, 2018, **6**, 16910.
6 Z. Bai, X. Wang, M. Zheng, O. Yue, M. Huang, X. Zou, B. Cui, L. Xie, S. Dong, J. Shang, G. Gong, A. M. Blocki, J. Guo and X. Liu, *Adv. Funct. Mater.*, 2023, **33**, 17.
7 Y. Luo, M. R. Abidian, J.-H. Ahn, D. Akinwande, A. M. Andrews, M. Antonietti, Z. Bao, M. Berggren, C. A. Berkey, C. J. Bettinger, J. Chen, P. Chen, W. Cheng, X. Cheng, S.-J. Choi, A. Chortos, C. Dagdeviren, R. H. Dauskardt, C.-a. Di, M. D. Dickey, X. Duan, A. Facchetti, Z. Fan, Y. Fang, J. Feng, X. Feng, H. Gao, W. Gao, X. Gong, C. F. Guo, X. Guo, M. C. Hartel, Z. He, J. S. Ho, Y. Hu, Q. Huang, Y. Huang, F. Huo, M. M. Hussain, A. Javey, U. Jeong, C. Jiang, X. Jiang, J. Kang, D. Karnaushenko, A. Khademhosseini, D.-H. Kim, I.-D. Kim, D. Kireev, L. Kong, C. Lee, N.-E. Lee, P. S. Lee, T.-W. Lee, F. Li, J. Li, C. Liang, C. T. Lim, Y. Lin, D. J. Lipomi, J. Liu, K. Liu, N. Liu, R. Liu, Y. Liu, Y. Liu, Z. Liu, Z. Liu, X. J. Loh, N. Lu, Z. Lv, S. Magdassi, G. G. Malliaras, N. Matsuhisa, A. Nathan, S. Niu, J. Pan, C. Pang, Q. Pei, H. Peng, D. Qi, H. Ren, J. A. Rogers, A. Rowe, O. G. Schmidt, T. Sekitani, D.-G. Seo, G. Shen, X. Sheng, Q. Shi, T. Someya, Y. Song, E. Stavrinidou, M. Su, X. Sun, K. Takei, X.-M. Tao, B. C. K. Tee, A. V.-Y. Thean, T. Q. Trung, C. Wan, H. Wang, J. Wang, M. Wang, S. Wang, T. Wang, Z. L. Wang, P. S. Weiss, H. Wen, S. Xu, T. Xu, H. Yan, X. Yan, H. Yang, L. Yang, S. Yang, L. Yin, C. Yu, G. Yu, J. Yu, S.-H. Yu, X. Yu, E. Zamburg, H. Zhang, X. Zhang, X. Zhang, X. Zhang, Y. Zhang, Y. Zhang, S. Zhao, X. Zhao, Y. Zheng, Y.-Q. Zheng, Z. Zheng, T. Zhou, B. Zhu, M. Zhu, R. Zhu, Y. Zhu, Y. Zhu, G. Zou and X. Chen, *ACS Nano*, 2023, **17**, 5211.
8 Q. Shi, Z. Sun, X. Le, J. Xie and C. Lee, *ACS Nano*, 2023, **17**, 4985.
9 S. Wang, Y. Yao, W. Deng, X. Chu, T. Yang, G. Tian, Y. Ao, Y. Sun, B. Lan, X. Ren, X. Li, T. Xu, L. Huang, Y. Liu, J. Lu and W. Yang, *ACS Nano*, 2024, **18**, 11183.
10 W. Yang, S. Liu, Z. Wang, H. Liu, C. Pan, C. Liu and C. Shen, *Nano Energy*, 2024, **127**, 109799.
11 W. Yang, H. Liu, H. Du, M. Zhang, C. Wang, R. Yin, C. Pan, C. Liu and C. Shen, *Sci. China Mater.*, 2023, **66**, 2829.
12 W. Yao, X. Lin, Z. Zhang, Q. Sun and H. Yang, *Adv. Mater. Technol.*, 2024, **9**, 2301983.
13 X. Wang, Y. Liu, H. Cheng and X. Ouyang, *Adv. Funct. Mater.*, 2022, **32**, 2200260.
14 Z. Wang, D. Xing, R. Yin, P. Zhan, C. Liu, C. Shen and H. Liu, *Appl. Mater. Today*, 2024, **38**, 102256.
15 T. Zhu, L. Liu, J. Huang, S. Li, Y. Lei, W. Cai, Y. Lai and H. Li, *J. Mater. Sci. Technol.*, 2023, **138**, 108.
16 Z. Dai, G. Chen, S. Ding, J. Lin, S. Li, Y. Xu and B. Zhou, *Adv. Funct. Mater.*, 2020, **31**, 2008574.
17 Q. Jin, Z. Liu, X. Ouyang, Y. Liu and X. Wang, *Chem. Eng. J.*, 2024, **488**, 150796.
18 Z. Wei, X. Li, X. Cai and X. Zhuang, *Chem. Eng. J.*, 2024, **487**, 150034.
19 W. Yao, Y. Yan, J. Sun, Z. Zhang, W. Sun, W. Huang, J. Cheng, H. Zhao, M. Xie, Q. Sun, G. Huang and X. Lin, *ACS Appl. Mater. Interfaces*, 2024, **16**, 6548.
20 Z. Dai, M. Lei, S. Ding, Q. Zhou, B. Ji, M. Wang and B. Zhou, *Exploration*, 2023, **4**, 20230046.
21 Y. Wei, X. Shi, Z. Yao, J. Zhi, L. Hu, R. Yan, C. Shi, H.-D. Yu and W. Huang, *npj Flexible Electron.*, 2023, **7**, 13.
22 H. Sun, Y. Bu, H. Liu, J. Wang, W. Yang, Q. Li, Z. Guo, C. Liu and C. Shen, *Sci. Bull.*, 2022, **67**, 1669.
23 X. Su, H. Li, X. Lai, Z. Chen and X. Zeng, *Adv. Funct. Mater.*, 2019, **29**, 1900554.
24 J. E. Mates, I. S. Bayer, J. M. Palumbo, P. J. Carroll and C. M. Megaridis, *Nat. Commun.*, 2015, **6**, 8874.
25 L. Li, Y. Bai, L. Li, S. Wang and T. Zhang, *Adv. Mater.*, 2017, **29**, 1702517.
26 S. Li, J. Tang, Y. Liu, J. Hua and J. Liu, *Compos. Sci. Technol.*, 2024, **249**, 110493.
27 Y. Bu, T. Shen, W. Yang, S. Yang, Y. Zhao, H. Liu, Y. Zheng, C. Liu and C. Shen, *Sci. Bull.*, 2021, **66**, 1849.
28 J. Wu, H. Li, X. Lai, Z. Chen and X. Zeng, *Chem. Eng. J.*, 2020, **386**, 123998.
29 J. Oh, S. G. Jang, S. Moon, J. Kim, H. K. Park, H. S. Kim, S. M. Park and U. Jeong, *Adv. Healthcare Mater.*, 2022, **11**, e2102703.
30 L. Xu, W. Wang, L. Zhang, D. Wang and A. Zhang, *ACS Appl. Mater. Interfaces*, 2022, **14**, 21623.
31 G. Tian, W. Deng, T. Yang, J. Zhang, T. Xu, D. Xiong, B. Lan, S. Wang, Y. Sun, Y. Ao, L. Huang, Y. Liu, X. Li, L. Jin and W. Yang, *Adv. Mater.*, 2024, **36**, 2313612.
32 J. Zhang, T. Yang, G. Tian, B. Lan, W. Deng, L. Tang, Y. Ao, Y. Sun, W. Zeng, X. Ren, Z. Li, L. Jin and W. Yang, *Adv. Fiber Mater.*, 2023, **6**, 133.
33 Q. T. Lai, X. H. Zhao, Q. J. Sun, Z. Tang, X. G. Tang and V. A. L. Roy, *Small*, 2023, **19**, 2300283.
34 H. Zhao, X. Ma, X. Xu, M. Cui, N. E. Stott, J. Zhu and J. Chen, *J. Mater. Chem. C*, 2024, **12**, 3203.
35 X. Zhang, Z. Li, C. Liu, J. Shan, X. Guo, X. Zhao, J. Ding and H. Yang, *Chem. Eng. J.*, 2023, **477**, 9.
36 T. Yang, W. Deng, X. Chu, X. Wang, Y. Hu, X. Fan, J. Song, Y. Gao, B. Zhang, G. Tian, D. Xiong, S. Zhong, L. Tang, Y. Hu and W. Yang, *ACS Nano*, 2021, **15**, 11555.
37 H. Zhu, Y. Huang, S. Zhang, S. Jin, X. Lou and F. Xia, *NPG Asia Mater.*, 2021, **13**, 47.
38 S. Jia, S. Deng, Y. Qing, G. He, X. Deng, S. Luo, Y. Wu, J. Guo, C. J. Carmalt, Y. Lu and I. P. Parkin, *Chem. Eng. J.*, 2021, **410**, 128418.
39 L. Wang, Y. Chen, L. Lin, H. Wang, X. Huang, H. Xue and J. Gao, *Chem. Eng. J.*, 2019, **362**, 89.
40 J. Y. Oh and Z. Bao, *Advanced Science*, 2019, **6**, 1900186.
41 J. Dong, D. Wang, Y. Peng, C. Zhang, F. Lai, G. He, P. Ma, W. Dong, Y. Huang, I. P. Parkin and T. Liu, *Nano Energy*, 2022, **97**, 107160.

42 J. Lin, X. Cai, Z. Liu, N. Liu, M. Xie, B. Zhou, H. Wang and Z. Guo, *Adv. Funct. Mater.*, 2020, **30**, 2000398.
43 P. Xiao, J. Gu, C. Wan, S. Wang, J. He, J. Zhang, Y. Huang, S.-W. Kuo and T. Chen, *Chem. Mater.*, 2016, **28**, 7125.
44 S. Wang, P. Xiao, Y. Liang, J. Zhang, Y. Huang, S. Wu, S.-W. Kuo and T. Chen, *J. Mater. Chem. C*, 2018, **6**, 5140.
45 S. Wang, S. Li, H. Wang, H. Lu, M. Zhu, X. E. Wu, H. Liang, X. Liang and Y. Zhang, *Adv. Funct. Mater.*, 2023, **33**, 2302687.